Resolving Conflicts During Human-Robot Co-Manipulation

Zaid Al-Saadi*
College of Engineering
Koc University, Istanbul, Turkey
zalsaadi13@ku.edu.tr

Yahya M. Hamad*
College of Engineering
Koc University, Istanbul, Turkey
yalqaysi13@ku.edu.tr

Yusuf Aydin
Faculty of Engineering
MEF University, Istanbul, Turkey
aydiny@mef.edu.tr

Ayse Kucukyilmaz
School of Computer Science
University of Nottingham, Nottingham, UK
ayse.kucukyilmaz@nottingham.ac.uk

Cagatay Basdogan
College of Engineering
Koc University, Istanbul, Turkey
cbasdogan@ku.edu.tr

ABSTRACT

This paper proposes a machine learning (ML) approach to detect and resolve motion conflicts that occur between a human and a proactive robot during the execution of a physically collaborative task. We train a random forest classifier to distinguish between harmonious and conflicting human-robot interaction behaviors during object co-manipulation. Kinesthetic information generated through the teamwork is used to describe the interactive quality of collaboration. As such, we demonstrate that features derived from haptic (force/torque) data are sufficient to classify if the human and the robot harmoniously manipulate the object or they face a conflict. A conflict resolution strategy is implemented to get the robotic partner to proactively contribute to the task via online trajectory planning whenever interactive motion patterns are harmonious, and to follow the human lead when a conflict is detected. An admittance controller regulates the physical interaction between the human and the robot during the task. This enables the robot to follow the human passively when there is a conflict. An artificial potential field is used to proactively control the robot motion when partners work in harmony. An experimental study is designed to create scenarios involving harmonious and conflicting interactions during collaborative manipulation of an object, and to create a dataset to train and test the random forest classifier. The results of the study show that ML can successfully detect conflicts and the proposed conflict resolution mechanism reduces human force and effort significantly compared to the case of a passive robot that always follows the human partner and a proactive robot that cannot resolve conflicts.

CCS CONCEPTS

- **Computer systems organization → Embedded and cyber-physical systems → Robotics**

* Both authors contributed equally to this research and are also with the Al-Khwarizmi College of Engineering – University of Baghdad.

This work is licensed under a Creative Commons Attribution-NonCommercial-ShareAlike International 4.0 License.

HRI '23, March 13–16, 2023, Stockholm, Sweden.
© 2023 Copyright is held by the owner/author(s).
ACM ISBN 978-1-4503-9964-7/23/03.
https://doi.org/10.1145/3568162.3576969

KEYWORDS

Physical human-robot interaction, conflict resolution, dyadic manipulation, machine learning, haptic features.

ACM Reference format:

Zaid Al-Saadi, Yahya M. Hamad, Yusuf Aydin, Ayse Kucukyilmaz, and Cagatay Basdogan. 2023. Resolving Conflicts During Human-Robot Co-Manipulation. In *Proceedings of the 2023 ACM/IEEE International Conference on Human-Robot Interaction (HRI '23), March 13–16, 2023, Stockholm, Sweden.* ACM, New York, NY, USA, 9 pages. https://doi.org/10.1145/3568162.3576969

1 INTRODUCTION

Collaborative robots have emerged during the last two decades due to the advancements in hardware (e.g., lightweight and safe design, built-in force/torque sensing) and software (e.g., user friendly interfaces, integrated artificial intelligence techniques). These enhancements have allowed robots to act near humans in activities through indirect interaction [1, 2] or within direct physical contact with humans [3, 4]. In object co-manipulation (see Figure 1), a collaborative robot can assist a human partner by bearing the weight of the jointly manipulated object and proactively guide the motion to lower human workload. However, if the motion intentions of the proactive robot are different from those of the human partner, conflicts may arise. If the robot has no means to resolve such conflicts, the task may become frustrating and exhausting for the human partner. Hence, a proactive robot should be aware of human intentions and act accordingly to perform the task naturally and effectively.

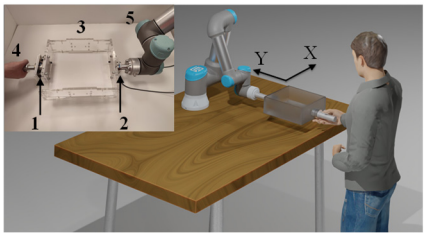


Figure 1: Human-robot co-manipulation scenario. Upper left figure shows the force sensors attached to the object for measuring the forces applied by human (1) and robot (2), the actual object being manipulated (3), the human hand (4), and the collaborative robot (5).

Consequently, in physical human-robot interaction (pHRI), a considerable amount of research has been directed toward detecting human intentions to regulate the interaction between humans and robots. Many of the earlier studies implemented rule-based methods, while more recent ones employed ML techniques. In this regard, we review the existing literature based on these two groups of studies.

In rule-based approaches, typically a set of rules are defined, based on thresholds over kinematic or kinetic interaction variables to detect human movement intentions. Wojtara et al. [5] implemented an interaction controller that allows a robot to follow the human partner's movement during a collaborative manipulation task based on the forces applied by the human on the object and the position of the human's grasp point. Other studies utilized velocity and human force [6], velocity and derivative of human force [7], velocity and acceleration [8], and velocity, human force, and its derivative [9] to predict human intentions to adjust parameters of an interaction controller for the robot during a collaborative manipulation task.

Rule-based approaches are also used to detect human intention to exchange roles, such as between leadership and followership. For example, Oguz et al. [10] and Kucukyilmaz et al. [11] proposed mechanisms for dynamic role exchanges between the human and the robot during collaborative haptic interaction tasks. In these studies, the authors inferred human intentions based on the forces applied on the manipulated object by the human to adjust the robot's role in the collaborative task. Later, Mörtl et al. [12] extended these methods to develop a rule-based strategy where robot and human partners could dynamically exchange their roles and adjust their contributions to the task based on the forces during a table co-manipulation task. Khoramshahi and Billard [13, 14] proposed dynamical system approaches in pHRI using human intended motion velocity to switch between different tasks, and to change robot's role between a stiff leader or a compliant follower to a human partner. Although these works demonstrate switching behaviors between active/passive roles, they do not perform harmony/conflict detection as done in this study.

The emergence of machine/deep learning techniques has encouraged researchers in pHRI to detect human intentions using data/model-driven approaches. Townsend et al. [15] trained an artificial neural network (ANN) to predict the future human velocity based on the past velocity and acceleration in a human-human co-manipulation task. This model was validated on a table carrying task executed by a human-robot dyad. Whitsell and Artemiadis [16] presented a controller that enables humans to take the leadership on any axis they desire while manipulating an object with a robot. They utilized force and torque data as inputs to a reinforcement learning algorithm to predict the value of future rewards to activate or deactivate the robot in the desired axis. Ge et al. [17] used the force, velocity, and position measured at the interaction point between the robot arm and human upper limb as inputs to an ANN model to estimate human motion intention, which is defined as the desired human upper limb trajectory. Guler et al. [18] trained an ANN classifier to detect the subtasks intended to be executed by the human operator during a collaborative drilling task. They adapted the interaction controller parameters based on the detected subtask to improve task efficiency. Lu et al. [19] utilized an LSTM model to estimate human motion intention as the desired trajectory based on human limb dynamics in a human-robot collaborative task. Based on this estimation, they used a reinforcement learning algorithm to adjust parameters of an interaction controller in real-time. Ly et al. [20] trained a Deep Q-Network to estimate human intentions to reach pre-learned motion trajectories and provided adaptive haptic guidance on a robotic sorting task. Chien et al. [21] used a fuzzy radial basis function impedance compensator to compute the hand compensation force that assists the robot in following an intended trajectory, estimated using an ANN model. Wang et al. [22] estimated human intention in human-robot hand-over tasks. They utilized an inertial measurement unit (IMU) and EMG sensors to measure arm motion along with muscle activity. These data were used as inputs to the extreme learning machine (ELM) algorithm to predict human hand-over intention. Sirintuna et al. [23] used EMG signals to detect the movement direction intended by human using an ANN model to constrain the movement directions using an interaction controller. Their approach reduces the motion errors during collaborative positioning with a robot.

The above studies focused on inferring human intentions to regulate the human-robot interactions. However, in the foreseeable future, as more sophisticated AI techniques are expected to be integrated into robotic systems, robots collaborating with humans are expected to have their own intentions. In such a scenario, if the intentions of a robot do not match those of the human, there will be motion conflicts [24]. For instance, consider a robot which proactively contributes to a co-manipulation task performed with a human partner. If the partners have a joint intention to push the manipulated object toward the same target, they will work harmoniously with minimal conflict. This harmonious interaction enables the human to spend less effort during the task. However, if the human changes the target by altering the direction of movement or stopping the motion before/after reaching the initial target location while the robot keeps moving toward it, conflicting behaviors will arise. Such behaviors create undesired interactions, which make the task tiring for the human partner unless the robot recognizes these conflicts and reacts to resolve them.

In our earlier works [25, 26], we defined a set of interaction behaviors that emerge from human partners' agreement or disagreement during collaborative manipulation of objects, akin to carrying a table together. ML classification models are shown to successfully distinguish between these behaviors using haptic and velocity data in [25] and haptic data solely in [26] as inputs to classification algorithms. Later, Kucukyilmaz and Issak [27] showed that these behaviors can be successfully recognized during real-time collaboration.

In this study, we aim to transfer the knowledge gained from human dyads [25, 26, 27] to a human-robot dyad. To this end, we trust that the identification and resolution of conflicts is a key skill that a robot needs to be equipped with to execute co-manipulation tasks with a human. We utilize features extracted from haptic data to build a random forest classifier that enables the robot to predict interaction behaviors and resolve conflicts when necessary. The

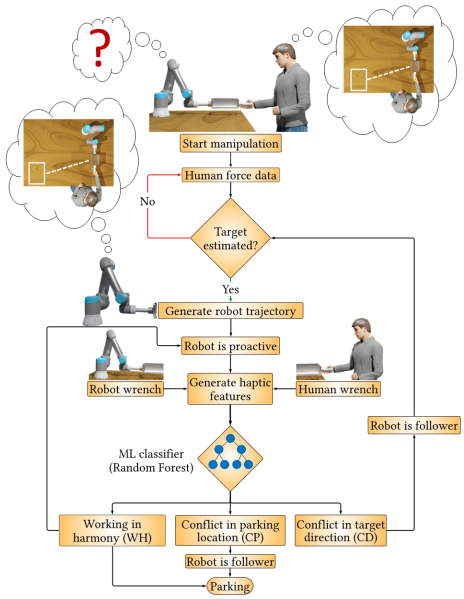


Figure 2: The flowchart of the proposed pHRI approach for co-manipulation of an object.

use of ML reduces reliance on task-specific thresholds, which are essential in rule-based approaches. In the current study, the robot contributes to the co-manipulation task proactively when the partners work in harmony, and follows the human when a conflict is detected between the partners' intentions. We show that the proposed approach significantly reduces the human force and effort compared to the case of a passive robot that always follows human partner and a proactive robot that cannot resolve conflicts.

2 APPROACH

In this paper, we focus on conflict-driven dyadic interaction patterns that typically emerge during co-manipulation. In our pHRI scenario, the human and the robot collaborate to jointly move an object (see Figure 1) toward a target location. Our approach detects interaction patterns using a random forest classifier, which is a supervised ML classification algorithm, and adapts the robot's role accordingly. Figure 2. presents a flowchart to summarize our approach: Initially, the robot passively follows the movements of the human based on the magnitude and direction of the forces applied by him/her, since it is not given the target location. Once the direction of human force vector settles (see Section 2.3), robot estimates an intended target location by intersecting a line in the direction of human force vector with a virtual boundary defined by a virtual circular workspace defined around the robot. An artificial potential field (APF) is generated to compute a trajectory for the robot to move the object toward the estimated target location. At this stage, the robot becomes proactive and moves the manipulated object collaboratively with the human partner. If the human changes the target during this manipulation, a conflict arises. We use a random forest ML model, trained with haptic-related features derived from the forces/torques (i.e., wrenches) applied on the object, to detect three interaction patterns:

1) WH: Working in Harmony: The partners agree on the target direction; hence, they move the object harmoniously.
2) CD: Conflict in target Direction: The partners face a conflict in movement direction as each aims at a different target location.
3) CP: Conflict in Parking location: The partners face a conflict in parking location since one of them aims to stop the motion of the object before or after the intended/estimated target location.

The random forest ML classifier detects these behaviors and notifies the interaction controller of the robot to generate a suitable response as shown in Figure 2. If WH pattern is detected, the controller maintains the proactive status of robot. On the other hand, if CD is detected, the controller switches the robot role to a follower until a new target location is determined and a new trajectory is generated. In CP, robot relinquishes its trajectory and acts as a follower to assist the human in parking the object. To avoid any jerky motion in CD and CP due to the switching between robot states, we gradually scale down the robot's attractive force in APF to zero once the robot turns from a proactive state to a passive state.

2.1 Hardware Setup

The setup used in our experiments consists of a UR5 collaborative robot, a box-shaped object made of plexiglass with dimensions of 30 cm × 25 cm × 10 cm and a weight of 2.5 kg, two force/torque (F/T) sensors (Mini45, ATI Inc.), and a computer screen to provide visual feedback for the participants. This setup physically couples the human and the robot through the manipulated object. One end of the object is rigidly connected to the robot via an F/T sensor to measure the wrenches applied by the robot. Human holds the object from the opposing end through an aluminum handle. A F/T sensor is attached to this handle to measure the human wrenches. All data is acquired at 125 Hz by an external DAQ card (USB-6343, National Instruments Inc.), connected to a personal computer.

2.2 Control Architecture

The control architecture utilized in this study is shown in Figure 3. An admittance controller regulates the interactions between the human and the robot. Initially, the target location is unknown to robot, which starts as a follower. At this stage, the ML classifier is not active, and only the human force, F_H, is fed to the admittance controller to generate the reference velocity V_{REF} for the robot's motion controller, which in turn, transmits torques to robot joints to move the object with velocity V. Once the target location is estimated by the robot based on the direction of human force, a trajectory is generated for the robot using the APF and the robot is pulled to the estimated target location with an attractive force F_{ATT} (we assume no obstacles in the environment, hence the repulsive force is always set to zero in this study). Here, the force applied by human partner F_H is added to F_{ATT} and the total force F_T is sent to the admittance controller. At this stage, ML classifier is active and utilizes the haptic-related features computed using the wrenches applied by human and robot (W_H and W_R) on the object, to predict the interaction pattern. If WH is detected, the robot contributes to the task proactively. On the other hand, if CD or CP is detected, the robot switches its role to a follower.

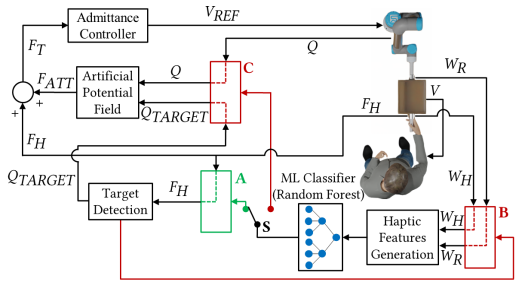


Figure 3: The control architecture utilized in our approach to regulate the harmonious and conflicting interactions between human and robot.

Role switching: Figure 3 includes logical commands to activate central input lines to turn on the data flow for blocks A, B, and C. The two-way switch S turns on block A while deactivating block C (i.e., robot is a follower), which is the starting phase of the motion in our approach. Similarly, if target location is determined, block B is activated; hence machine learning is involved. Consequently, switch S, which works based on the classifier decision, activates block C whenever WH pattern is detected. On the other hand, if the ML classifier observes one of the conflicting patterns (CD or CP), block C is deactivated by switch S, and the robot is a follower again.

Admittance Controller: The transfer function model of the admittance controller utilized in this study is similar to that in [9]:

$$Y(s) = \frac{V_{REF}(s)}{F_T(s)} = \frac{K_A}{\tau_A s + 1} \tag{1}$$

where, K_A and τ_A are the admittance gain and time constant, respectively, $V_{REF}(s)$ and $F_T(s)$ are respectively the Laplace transformations of the reference velocity and the total force.

2.3 Trajectory Generation

We utilize an APF (artificial potential field) to generate a trajectory for the robot, to be used when it proactively cooperates with the human partner. In APF, the total potential field $U(Q)$ is made of an attractive, $U_{ATT}(Q)$, and a repulsive, $U_{REP}(Q)$, field [28]. In our scenario, there are no physical obstacles in the environment, hence we ignore the repulsive field. However, even if there were obstacles, the proposed paradigm would have worked without needing any modifications: The human could perceive the environment and direct the motion to avoid obstacles, while the robot reacts to detected conflicts.

The total force, which defines the robot's contribution to the task, is calculated as the negative gradient of the total potential field, $F_{ATT} = -\nabla U(Q) = -\nabla U_{ATT}$. This attractive force is set at its maximum value when the robot is fully proactive, and gradually reduces to zero as it reaches the target.

To implement the APF, the position of the target Q_{TARGET} should be known by the robot. However, estimating the intended target location at the very beginning of the movement, which is only known by human, is not trivial. In our approach, initially, robot has no prior information about the target location; hence it starts the task as a follower while human guides it toward the target by applying forces to the manipulated object. Once the direction of the human force vector settles toward a specific direction, robot utilizes this direction to estimate the target location by intersecting the vector of human force with a virtual circular task boundary within the robot workspace, centered around the robot base frame. To decide that the human's forces settle on a direction, we first measure the angle (θ) between the human force vector and the x-axis of robot. Then, we select a sliding buffer of size n for the measured data and compute the mean of the absolute differences between the angles in this buffer and their average. When this mean value is less than a threshold value (i.e., $(\Sigma_{i=1}^{n} |\theta_i - \theta_{AVE}| / n) < \theta_{THR}$), we consider that the human force vector settled in the desired direction without considerable deviation. Note that when human changes the target location by altering the movement direction during the manipulation while robot is still active and moves toward the initial target, conflict in target direction (i.e., CD) emerges. Once robot detects this conflict, it leaves its own trajectory and follows the human passively until it can estimate the new target location and generate a new trajectory.

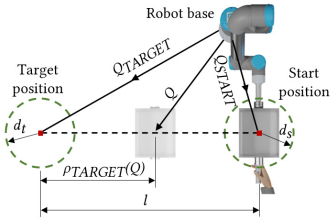


Figure 4: The parameters used for implementing the hybrid formulation for APF.

To avoid high attractive forces far from the target, we utilize a hybrid APF that uses quadratic potentials near the target and a conic formula when farther away as illustrated in Figure 4 [28]:

$$F_{ATT} = \begin{cases} -\xi (Q - Q_{TARGET}) & \text{if } \rho_{TARGET}(Q) \le d_t \\ -d_t\, \xi \dfrac{(Q - Q_{TARGET})}{\rho_{TARGET}(Q)} & \text{if } l - d_s > \rho_{TARGET}(Q) > d_t \\ -d_t\, \xi \dfrac{(Q - Q_{TARGET})}{\rho_{TARGET}(Q)}\, m & \text{if } \rho_{TARGET}(Q) \ge l - d_s \end{cases} \tag{2}$$

where ξ is a positive constant scaling factor, Q and Q_{TARGET} are respectively the current and target position vectors of the object with respect to the robot base frame, d_t is a positive constant to define a catchment area around the target for switching between quadratic and conic formulas, and $\rho_{TARGET}(Q)$ is the Euclidean distance to target $\|Q - Q_{TARGET}\|$. To prevent the attractive force from being set to its maximum value, $F_{ATT} = d_t\, \xi$, at the beginning of the task, which would cause a jerky motion, we introduced three new variables as shown in Figure 4: $l = \|Q_{START} - Q_{TARGET}\|$ is the Euclidean distance between the object's starting position vector, Q_{START} and the estimated target, d_s is a distance threshold around Q_{START}, and $m = ((d_s - \rho_{START}(Q)) / l) + (\rho_{START}(Q)) / d_s$ is a scaling constant, where $\rho_{START}(Q) = \|Q - Q_{START}\|$.

3 EXPERIMENTS

In order to train and validate our ML classifier, we designed and implemented two sets of pHRI experiments:

1) Training Experiments: These experiments were designed to train and test the ML time-series classifier, relying on haptic

features for distinguishing between the human-robot interaction behaviors.

2) Validation Experiments: These experiments were designed to investigate the potential benefits of the proposed ML approach in comparison to two other approaches.

All experiments utilized the same setup shown in Figure 1. The object manipulations mainly involved translation and performed in the xy plane. The experimental study was approved by the Ethical Committee for Human Participants of Koc University. The values of the parameters used in the implementation were selected as; $K_A = 0.0167$, $\tau_A = 0.054$, $n = 30$, $d_t = 8$ cm, $d_s = 4$ cm, $\xi = 125$, and $\theta_{THR} = 0.08$ rad.

3.1 Training Experiments

3.1.1 Training Scenarios. The objective in designing the training scenarios was to collect haptic data to train a classifier model that can effectively distinguish between different interaction patterns (WH, CD, CP). To this end, 16 different manipulation scenarios, listed in Table 1, were introduced by covering as many different combinations of interaction behaviors as possible without being too exhaustive. In these training scenarios (TS), human and robot collaborate to move the object from the starting location to one of the target locations shown in Figure 5 (A, B, C, D, E, F). In designing these scenarios, we intentionally created harmonious and conflicting patterns by assigning a specific target location for the robot and hence a trajectory to follow, regardless of the human partner's target location. As a result, harmonious/conflicting interaction patterns resulted from the agreement/disagreement between the partners.

Table 1: Training scenarios and the expected interaction behaviors.

Training scenario (TS)	Robot target	Human target		Expected behavior
		Initial	Final	
TS1	B	B	B	WH
TS2	E	E	E	WH
TS3	B	E	E	CD
TS4	E	B	B	CD
TS5	B	A	A	WH, CP
TS6	B	C	C	WH, CP
TS7	E	D	D	WH, CP
TS8	E	F	F	WH, CP
TS9	B	B	F	WH, CD
TS10	E	E	B	WH, CD
TS11	E	B	D	CD, WH, CP
TS12	E	B	F	CD, WH, CP
TS13	B	E	A	CD, WH, CP
TS14	B	E	C	CD, WH, CP
TS15	E	B	E	CD, WH
TS16	B	E	B	CD, WH

To put things into context, consider training scenario 8 in Table 1, where both the human and the robot have the same target direction but different locations; therefore, they are expected to work in harmony (WH) initially to move the object toward that direction. However, as the human's scenario requires him/her to park the object (at target F in Figure 5) before the robot's target (target E in Figure 5), they face a conflict in parking location, CP.

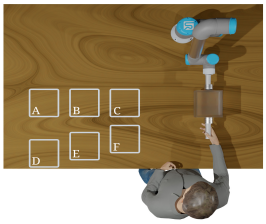


Figure 5: Scenarios used in training experiments.

3.1.2 Participants and Protocol. The training experiments were performed with 8 subjects (2 females and 6 males with an average age of 26.25 ± 4.2 SD). Prior to the experiment, subjects were instructed about the experimental procedure. They were not aware of the robot's target and were explicitly instructed to move the object toward their own targets regardless of robot's behavior. Subjects performed the task by following the text instructions and visual images displayed on a computer screen, and the software sounds played during the experiment. To familiarize themselves with the setup, all subjects performed one manipulation trial involving harmonious collaboration (WH) with the robot. Thereafter, each subject performed the scenarios listed in Table 1 in four separate sessions with 5 minutes break between the sessions. Each subject performed 32 trials, where each scenario repeated twice. The order of the scenarios was randomized in each session, while the order for all subjects was the same.

Subjects started the experiment by grasping the object from their handle while facing the robot handling the object from the other side by its end effector. To provide visual feedback to the subjects, initial and target locations were displayed on the computer screen as static 2D rectangles in white color while the current location of the manipulated object was displayed as a moving 2D rectangle in pink. A message was displayed on the screen along with a distinct software sound to notify subjects to start the task. During the task, if the scenario involved a change in target location, the new target location was updated immediately on the screen to notify the subject. When the subject reached the target, the color of the rectangle at the target changed to green to notify the subject, and after staying at the target for 2 seconds, a message appeared on the screen along with a distinct beep to inform the subject about successfully parking the object.

3.1.3 Haptic Features and Classifier Design. The raw haptic data (i.e., wrenches applied by human and robot) collected during the training experiments are annotated and segmented based on the expected behaviors listed in Table 1 by following the procedure employed in [26]. As demonstrated in this work, the features extracted from the haptic data alone are sufficient to distinguish between different interaction patterns. We utilize the haptic features, originally suggested by Noohi and Žefran [29] and extended by Al-Saadi et al. [26] to train our random forest ML classifier. We briefly mention them here for the sake of discussion, but the details are available in [26].

Consider Figure 6, where F_H, F_R, and F_{SUM} are the forces applied on an object by the human and the robot, and the summation of these forces, respectively. That is:

$$F_{SUM}(t) = F_H(t) + F_R(t) \quad (3)$$

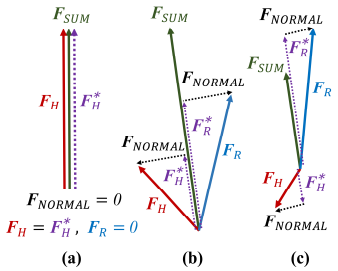


Figure 6: Force decomposition.

The effective forces of human F_H^* and robot F_R^* that contribute to the task are calculated as the projection of partners' forces on F_{SUM}:

$$F_H^*(t) = \alpha\, F_{SUM}(t) \quad (4)$$

$$F_R^*(t) = \beta\, F_{SUM}(t) \quad (5)$$

where t is the time step and $\alpha + \beta = 1$. The forces that are perpendicular to F_{SUM} (i.e., F_{NORMAL} in Figure 6) do not contribute to the task and are canceled out.

Based on this force decomposition, five force-related features were introduced: individual force efficiencies $M^F_{E_K}$, team force efficiency M^F_{TE}, negotiation force efficiency M^F_{NE}, and similarity of forces M^F_S. In addition, five additional torque-related features were introduced in [26]: individual torque efficiencies $M^\tau_{E_K}$, team torque efficiency M^τ_{TE}, negotiation torque efficiency M^τ_{NE}, and similarity of torques M^τ_S. Note that the subscript K in $M^F_{E_K}$ and $M^\tau_{E_K}$ refers to either human (H) or robot (R), while the superscripts F and τ refer to force and torque-related features, respectively.

In [26], we showed that analyzing the task in different movement planes resulted in more informative features than analyzing it in 6-DoF space. For that, we performed the force/torque decomposition in the three principal movement planes, *xy*, *xz*, and *yz*. This resulted with 30 wrench-related features (10 wrench-related features × 3 planes) that are used as inputs into our classifier. We utilized a random forest algorithm to train our time-series classifier model to discriminate between the interaction patterns. Random forest is a supervised learning algorithm used for both regression and classification. In classification, it constructs a multitude of decision trees and outputs the class selected by most of them. Python Scikit-Learn package was utilized for the implementation of the algorithm [30]. The number of trees in the random forest was set to 100 while the maximum depth of the trees was unconstrained.

We split the dataset into two distinct sets: training and test. To train the classification model, we used the data coming from 24 trials of each subject and used the remaining 8 trials for testing. Since there were 8 subjects, the total number of trials for training and testing were 192 (75%) and 64 (25%), respectively. We achieved a classification accuracy of 88.82% and a BER of 0.11 after cross-validation. Figure 7 shows the confusion matrix.

3.2 Validation Experiments

To evaluate the performance of our proposed approach, we implemented another set of experiments utilizing the same setup

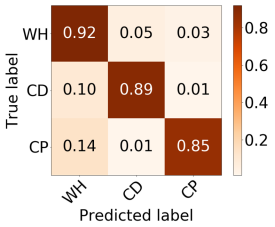


Figure 7: Confusion matrix for classifier trained with haptic feature set.

and scenarios. Recalling the co-manipulation example discussed in the introduction section, where the robot acts either as a follower or interacts proactively with human, we considered 3 experimental conditions (C1, C2, and C3). The first condition, C1, implements a simple leader-follower model where the robot is passive and always follows the human. In C2, the robot has a fixed target location and follows a trajectory based on the APF, regardless of the agreement/disagreement with human partner. In C2, the robot assists the human partner (i.e., contributes to the task) if they have the same target. Nevertheless, when they are given different target locations, they display conflicting behaviors, which cannot be resolved. Finally, C3 utilizes our approach of integrating the APF with the ML classifier for conflict resolution.

Three different experimental scenarios (ES1, ES2, and ES3) were considered for the validation experiments (Figure 8). In ES1, human and robot work in harmony (WH) to transport the object to a target position (point B), while in ES2, the target location changes suddenly from location B to location E, causing a conflict in movement direction (CD). Finally, in ES3, the target location suddenly changes from location B to location C, causing a conflict in parking location (CP).

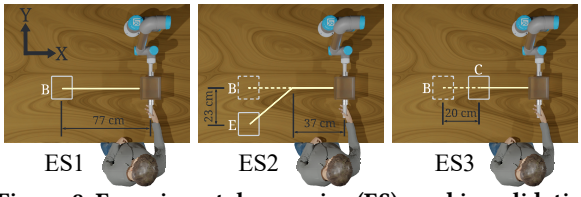


Figure 8: Experimental scenarios (ES) used in validation experiments.

Six subjects, with an average age of 25.5 ± 4.4 SD, participated in this experiment. Each experimental condition (C1, C2, and C3) was repeated twice for each experimental scenario (ES1, ES2, and ES3). Hence, the total number of trials performed by each subject was 18, which were completed in two sessions with 5 minutes break between the sessions. The order of the experimental conditions and scenarios was randomized in each session while the same order was displayed to each participant.

3.2.1 Results and Discussions

3.2.1.1 Force Profiles and Classifier Performance. Figure 9 represents the force profiles of a representative dyad (a human and a robot) for ES1, ES2, and ES3 under C3 (our approach) in tandem with the decisions taken by the classifier. We concentrated on the forces applied in the *xy* plane, which is the plane of most movements in our experiment. In all plots, subscripts H and R stand for human and robot, respectively. The

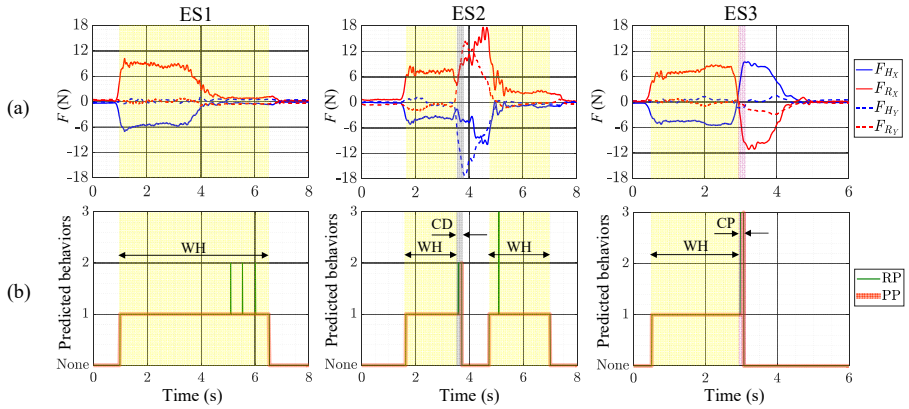


Figure 9: (a) Forces profiles of a human subject (blue) and robot (red), and (b) the raw predictions (RP) by ML and the processed predictions (PP) after filtering for the experimental scenarios ES1, ES2, and ES3 under our proposed approach (C3). Subscripts *H* and *R* stand for human, robot, respectively. The predicted values 1, 2, and 3 stand for WH, CD, and CP interaction behaviors, respectively, while "None" stands for the periods where ML is inactive, and the robot is follower.

blue and red lines in Figure 9a represent the forces applied by human and robot, respectively (please note that all forces were presented with respect to the manipulated object frame), while Figure 9b depicts the raw predictions RP (green vertical lines) and processed predictions PP (orange line) of the ML classifier. As shown in Figure 9b, the classifier successfully predicted the interaction behaviors in all experimental scenarios. Moreover, the classifier was able to predict the conflicting behaviors (i.e., CD in ES2 and CP in ES3), which occurred for short periods of time only, and instructed the controller to resolve the conflicts by switching the robot to a follower state. Prior to sending the classifier decision to the controller, a voting buffer was implemented:

Voting buffer: This buffer uses raw predictions within a window of 20 samples, with an overlap of 10 samples between each buffer, and outputs the most frequent prediction in the buffer. The behavior predictions are processed every 10 samples. Using this buffer eliminates instantaneous misclassifications due to the sudden and unintentional movements. For instance, in Figure 9b, some patterns were misclassified initially (i.e., a CP in ES2 and some CDs in ES1), but these were filtered out by the voting buffer.

By inspecting the interaction behaviors in Figure 9, we observed that they produced highly complex force profiles though the object manipulations were translational (no rotations) and mainly performed in the xy plane. For example, the yellow-colored shaded areas in Figure 9 correspond to WH behavior, in which the partners harmoniously translated the object toward the target. One anticipates that partners perform the manipulation by exerting forces in the same direction of the movement during this type of interaction. However, when the force profiles in Figure 9a are inspected carefully, one observes that only human partner applies forces in the direction of the movement while the forces applied by robot are in the opposite direction. The reason for this mismatch is due to the delay in the reaction times of the partners to each other's actions as also observed in human dyads [26].

The grey-colored shaded area in Figure 9 corresponds to CD behavior, in which the partners disagreed on the target direction. This behavior occurred in ES2 scenario: a new target location (location E in Figure 8) was suddenly displayed to the subject, and he/she started to apply forces in the negative y-axis to move the object toward the new target. As the robot was still actively moving toward the original target location (location B in Figure 8), it resisted human movement, which resulted in the opposing forces applied by the partners along the y-axis. By inspecting the force patterns during this behavior, we observed that they changed in both x and y directions, although the new target position deviated from the initial one along the y-direction only.

Finally, in CP behavior (the pink-colored shaded area in Figure 9), the subject and the robot were given the same target location of B as shown in ES3 in Figure 9, but the subject was instructed later to park the object suddenly at location C prior to reaching the original target location at B. Subject applied forces in opposite direction to the movement (along x-axis) to park the object at location C, as clearly shown in Figure 9a for ES3 (see the change in the direction of forces in the pink shaded region). However, since the robot was moving the object toward B, it applied forces opposite to the direction of forces applied by the subject.

The observations above reveal the complexity of the force signals though the task was implemented in 2D. This infers that generating rules based on force signals to distinguish between these behaviors is not straightforward, especially when the task is conducted in 6D. Hence, the ML approach proposed in this paper has more generalization potential to identify similar behaviors.

3.2.1.2 Task Performance Under C1, C2, and C3. We used the following metrics [9, 31] to evaluate the task performance of the subjects: the average velocity of the object ($V^{\text{AVE}} = 1/(t_f - t_i)\int_{t_i}^{t_f}|V(t)|\,dt$), average force applied by subject ($F_H^{\text{AVE}} = 1/(t_f - t_i)\int_{t_i}^{t_f}|F_H(t)|\,dt$), average power consumed by the human ($P^{\text{AVE}} = 1/(t_f - t_i)\int_{t_i}^{t_f}|F_H(t)V(t)|\,dt$), and the task completion time (TCT). Here, t_i and t_f are the timestamps when the object velocity just exceeded 2% of the maximal velocity (denoting the start of the trial) and the ending time of the trial, respectively. TCT was computed as $t_f - t_i$.

Figure 10 presents the means and standard errors of means of the performance metrics of the subjects under each experimental

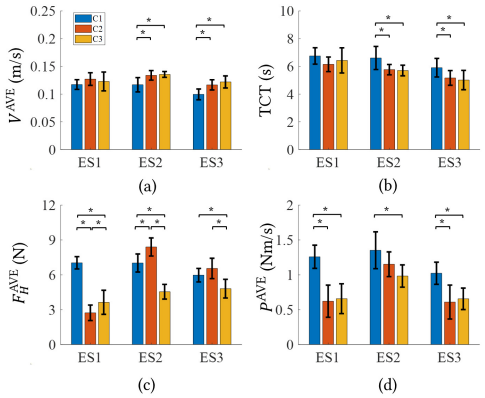


Figure 10: Mean values of the performance metrics for three experimental scenarios ES1, ES2, and ES3 under three different experimental conditions C1, C2, and C3. Error bars are the standard deviations of means and horizontal bracket with * on top indicates statistically significance pairwise comparisons with $p = 0.05$.

condition (C1, C2, and C3) for each scenario. We performed a one-way ANOVA with Tukey corrected post-hoc tests to examine the effects of the experimental conditions on the performance metrics.

Figure 10a (10b) shows that V^{AVE} (TCT) under C2 and C3 were significantly higher (lower) than that of C1 in both ES2 and ES3. Although V^{AVE} (TCT) under C2 and C3 were higher (lower) than that of C1 in ES1, the difference was not statistically significant. In addition, the differences in V^{AVE} and TCT between C2 and C3 were not significant in any experimental scenario.

In Figure 10c, we observe that the average forces applied by subjects F_H^{AVE} under C3 (our proposed approach) were significantly lower than those of C1 and C2 in both ES2 and ES3, and lower than that of C1 in ES1. In addition, F_H^{AVE} under C2 was lower than those of C1 and C3 in ES1. This shows that the ML classifier in our proposed approach (C3) successfully resolved the conflicts between human and robot, and hence reduced the forces exerted by human to change the direction of movement or parking location. Additionally, F_H^{AVE} under C2 was higher than those of C1 in both ES2 and ES3. Although the APF utilized in C2 reduced the task completion time compared to C1, it caused the subjects to exert more force during the conflicting scenarios in ES2 and ES3.

Figure 10d shows that subjects spent less effort P^{AVE} under C2 and C3 compared to that under C1 due to the benefit of utilizing APF, especially in ES1. Moreover, when the conflict was stronger, as in ES2, C3 led to less effort than that of C2, thanks to our ML model in resolving the conflict. The results on P^{AVE} showed that the conflicts in parking (ES3) were more easily (with less effort) resolved than the conflicts in changing direction (ES2).

In summary, our proposed approach C3 resolved the conflicts between the partners effectively, allowing subjects to exert less force than those under C1 and C2. However, in ES1, where no conflict happened, we can see that F_H^{AVE} under C3 was higher than that of C2. This is because the robot in C2 was active through the whole task, while in C3, human needs to apply forces to guide the robot as it starts the task as a follower. Although subjects applied less force under C3, they translated the object with higher velocities and lower TCT (particularly compared to those under C1). The results of the experiments show that our approach (C3) reduces the average force applied by subjects by 42.65% and 30.6% compared to those under C1 and C2, respectively. Moreover, the average power spent by the subjects under C3 was reduced by 46.27% and 4.94% compared to those of C1 and C2, respectively.

4 CONCLUSION

We proposed an approach that allows the robot to proactively interact with a human partner based on the time-series classification of the interaction behaviors that arise while executing a collaborative task. During these interactions, conflicts may naturally arise if the partners have different movement intentions. To resolve these conflicts, we argue that it is important to study the dyadic interaction behaviors rather than the individual behavior of human partner. Moreover, we show that the features derived from haptic data alone are sufficient to detect these conflicts. These features were used to train a random forest classifier that differentiates between the interaction patterns.

To demonstrate our approach, we designed a pHRI experiment where both human and robot collaborated to manipulate an object. Experimental scenarios that involve partners work in harmony and conflict with each other in movement direction and parking location were designed to test the efficacy of the proposed approach. The results showed that our ML classifier successfully recognized the interaction behaviors that emerged during those scenarios and instructed the robot to take proper action accordingly. Hence, the robot was able to adapt its behavior to act as a follower when there was a conflict or contribute to the task proactively when the dyad was working in harmony. As a result, the conflicts between human and robot during the manipulation were accommodated effectively and the subjects performed the task with lower effort.

Our current experimental scenarios involved translational manipulations of an object in 2D space. As a future work, we aim to extend our approach to more complex scenarios involving object manipulations in 6D space. In particular, we would like to show that a rule-based approach (e.g., defining some rules based on force magnitudes/thresholds) cannot successfully detect conflicts in such complex manipulation scenarios, or the same rules cannot be applied easily to other manipulation scenarios involving different sub-tasks or objects having different shape, weights or material properties (e.g., elastic objects). Additionally, we would like to design a questionnaire, similar to that done in [32], to measure the perceptions of human subjects participating in our experiments about their sense of interaction with the robot under different experimental conditions and scenarios. We are interested in quantifying the degree of conflict that they subjectively feel in the presence of a proactive robot and how much of our approaches help humans to resolve such conflicts.

ACKNOWLEDGEMENTS

This work is partially funded by UKRI and CHIST-ERA (HEAP: EP/S033718/2; Horizon: EP/T022493/1; TAS Hub: EP/V00784X).

REFERENCES

[1] Anca D. Dragan and Siddhartha S. Srinivasa, 2013. A policy-blending formalism for shared control. *The International Journal of Robotics Research*, vol. 32, issue 7, pp. 790-805, (2013). https://doi.org/10.1177/0278364913490324

[2] Javdani Shervin, Henny Admoni, Stefania Pellegrinelli, Siddhartha S. Srinivasa, and J. Andrew Bagnell, 2018. Shared autonomy via hindsight optimization for teleoperation and teaming. *The International Journal of Robotics Research*, vol.37, issue 7, pp. 717-742, (2018). https://doi.org/10.1177/0278364918776060

[3] Francesco Semeraro, Alexander Griffiths, and Angelo Cangelosi, 2022. Human-robot collaboration and machine learning: a systematic review of recent research. arXiv:2110.07448v4, (2022). https://doi.org/10.48550/arXiv.2110.07448

[4] Arash Ajoudani, Andrea Maria Zanchettin, Serena Ivaldi, Alin Albu-Schäffer, Kazuhiro Kosuge, and Oussama Khatib, 2018. Progress and prospects of the human–robot collaboration. *Autonomous Robots*, vol. 42, pp. 957–975, (2018). https://doi.org/10.1007/s10514-017-9677-2

[5] Tytus Wojtara, Masafumi Uchihara, Hideyuki Murayama, Shingo Shimoda, Satoshi Sakai, Hideo Fujimoto, and Hidenori Kimura, 2009. Human–robot collaboration in precise positioning of a three-dimensional object. *Automatica*, vol. 45, no. 2, pp. 333 – 342, (2009). https://doi.org/10.1016/j.automatica.2008.08.021

[6] Gitae Kang, Hyun Seok Oh, Joon Kyue Seo, Uikyum Kim, and Hyouk Ryeol Choi, 2019. Variable Admittance Control of Robot Manipulators Based on Human Intention. In *IEEE/ASME Transactions on Mechatronics*, vol. 24, no. 3, pp. 1023-1032, (June 2019). https://doi.org/10.1109/TMECH.2019.2910237

[7] Yusuf Aydin, Nasser Arghavani and Cagatay Basdogan, 2014. A New Control Architecture for Physical Human-Robot Interaction Based on Haptic Communication. *9th ACM/IEEE International Conference on Human-Robot Interaction (HRI)*, pp. 122-123, (2014). http://dx.doi.org/10.1145/2559636.2563682

[8] Alexandre Lecours, Boris Mayer-St-Onge, and C. Gosselin, 2012. Variable admittance control of a four-degree-of-freedom intelligent assist device. *IEEE International Conference on Robotics and Automation*, pp. 3903-3908, (2012). https://doi.org/10.1109/ICRA.2012.6224586

[9] Yahya M. Hamad, Yusuf Aydin, and Cagatay Basdogan, 2021. Adaptive Human Force Scaling via Admittance Control for Physical Human-Robot Interaction. In *IEEE Transactions on Haptics*, vol. 14, no. 4, pp. 750-761, (2021). https://doi.org/10.1109/TOH.2021.3071626

[10] S. Ozgur Oguz; Ayse Kucukyilmaz; Tevfik Metin Sezgin; Cagatay Basdogan, 2012. Supporting Negotiation Behavior with Haptics-Enabled Human-Computer Interfaces. In *IEEE Transactions on Haptics*, vol. 5, no. 3, pp. 274-284, (2012). https://doi.org/10.1109/TOH.2012.37

[11] Ayse Kucukyilmaz, Tevfik Metin Sezgin, and Cagatay Basdogan, 2013. Intention Recognition for Dynamic Role Exchange in Haptic Collaboration. In *IEEE Transactions on Haptics*, vol. 6, no. 1, pp. 58-68, (First Quarter 2013). https://doi.org/10.1109/TOH.2012.21

[12] Alexander Mörtl, Martin Lawitzky, Ayse Kucukyilmaz, Metin Sezgin, Cagatay Basdogan, and Sandra Hirche, 2012. The role of roles: Physical cooperation between humans and robots. *The International Journal of Robotics Research*, vol. 31, no.13, pp. 1656–1674, (2012). https://doi.org/10.1177/0278364912455366

[13] Mahdi Khoramshahi and Aude Billard, 2019. A dynamical system approach to task-adaptation in physical human–robot interaction. *Autonomous Robots*, 43, pp. 927–946, (2019). https://doi.org/10.1007/s10514-018-9764-z

[14] Mahdi Khoramshahi and Aude Billard, 2020. A dynamical system approach for detection and reaction to human guidance in physical human–robot interaction. *Autonomous Robots*, 44, pp. 1411–1429, (2020). https://doi.org/10.1007/s10514-020-09934-9

[15] Eric C. Townsend, Erich A Mielke, David Wingate, and Marc D. Killpack, 2017. Estimating human intent for physical human-robot co-manipulation. (2017). https://doi.org/10.48550/arXiv.1705.10851

[16] Bryan Whitsell and Panagiotis Artemiadis, 2017. Physical Human–Robot Interaction (pHRI) in 6 DOF With Asymmetric Cooperation. In *IEEE Access*, vol. 5, pp. 10834-10845, (2017). https://doi.org/10.1109/ACCESS.2017.2708658

[17] Shuzhi Sam Ge, Yanan Li, and Hongsheng He, 2011. Neural-network-based human intention estimation for physical human-robot interaction. *8th International Conference on Ubiquitous Robots and Ambient Intelligence (URAI)*, pp. 390-395, (2011). https://doi.org/10.1109/URAI.2011.6145849

[18] Berk Guler, Pouya P. Niaz, Alireza Madani, Yusuf Aydin, and Cagatay Basdogan, 2022. An adaptive admittance controller for collaborative drilling with a robot based on subtask classification via deep learning. *Mechatronics*, 86:102851, (2022). https://doi.org/10.1016/j.mechatronics.2022.102851

[19] Weifeng Lu, Zhe Hu, and Jia Pan, 2020. Human-Robot Collaboration using Variable Admittance Control and Human Intention Prediction. *IEEE 16th International Conference on Automation Science and Engineering (CASE)*, pp. 1116-1121, (2020). https://doi.org/10.1109/CASE48305.2020.9217040

[20] Kim Tien Ly, Mithun Poozhiyil, Harit Pandya, Gerhard Neumann, and Ayse Kucukyilmaz. 2021. Intent-Aware Predictive Haptic Guidance and its Application to Shared Control Teleoperation. *IEEE International Conference on Robot & Human Interactive Communication (RO-MAN)*, pp. 565-572, (2021). https://doi.org/10.1109/RO-MAN50785.2021.9515326

[21] Shih-Hsuan Chien, Jyun-Hsiang Wang, and Ming-Yang Cheng, 2021. Robotic Assistance for Physical Human–Robot Interaction Using a Fuzzy RBF Hand Impedance Compensator and a Neural Network Based Human Motion Intention Estimator. In *IEEE Access*, vol. 9, pp. 126048-126057, (2021). https://doi.org/10.1109/ACCESS.2021.3111875

[22] Weitian Wang, Rui Li, Yi Chen, and Yunyi Jia. 2018. Human Intention Prediction in Human-Robot Collaborative Tasks. In *Companion of the 2018 ACM/IEEE International Conference on Human-Robot Interaction (HRI '18).* Association for Computing Machinery, New York, NY, USA, pp. 279–280, (2018). https://doi.org/10.1145/3173386.3177025

[23] Doganay Sirintuna, Idil Ozdamar, Yusuf Aydin, and Cagatay Basdogan, 2020. Detecting Human Motion Intention during pHRI Using Artificial Neural Networks Trained by EMG Signals. *29th IEEE International Conference on Robot and Human Interactive Communication (RO-MAN)*, pp. 1280-1287, (2020). https://doi.org/10.1109/RO-MAN47096.2020.9223438

[24] Franziska Babel, Johannes M. Kraus, and Martin Baumann, 2021. Development and Testing of Psychological Conflict Resolution Strategies for Assertive Robots to Resolve Human-Robot Goal Conflict. *Front Robot AI*, Vol. 7, Article 591448, (2021). https://doi.org/10.3389/frobt.2020.591448

[25] Cigil Ece Madan, Ayse Kucukyilmaz, Tevfik Metin Sezgin, and Cagatay Basdogan, 2015. Recognition of haptic interaction patterns in dyadic joint object manipulation. *IEEE Transactions on Haptics*, vol. 8, no. 1, pp. 54–66, (2015). https://doi.org/10.1109/TOH.2014.2384049

[26] Zaid Al-Saadi, Doganay Sirintuna, Ayse Kucukyilmaz, and Cagatay Basdogan, 2021. A Novel Haptic Feature Set for the Classification of Interactive Motor Behaviors in Collaborative Object Transfer. In *IEEE Transactions on Haptics*, vol. 14, no. 2, pp. 384-395, (2021). https://doi.org/10.1109/TOH.2020.3034244

[27] Ayse Kucukyilmaz, and Illimar Issak, 2020. Online identification of interaction behaviors from haptic data during collaborative object transfer. *in IEEE Robotics and Automation Letters*, vol. 5, no. 1, pp. 96-102, (Jan. 2020). https://doi.org/10.1109/LRA.2019.2945261

[28] Oussama Khatib, 1986. Real-time obstacle avoidance for manipulators and mobile robots. In *Proceedings of the IEEE Conference on Robotics and Automation*, pp. 500-505, (1986). https://doi.org/10.1109/ROBOT.1985.1087247

[29] Ehsan Noohi and Miloš Žefran, 2014. Quantitative measures of cooperation for a dyadic physical interaction task. In *IEEE-RAS International Conference on Humanoid Robots*, pp. 469–474, (2014). https://doi.org/10.1109/HUMANOIDS.2014.7041403

[30] Fabian Pedregosa, Gaël Varoquaux, Alexandre Gramfort, Vincent Michel, Bertrand Thirion, Olivier Grisel, Mathieu Blondel, Peter Prettenhofer, Ron Weiss, Vincent Dubourg, Jake Vanderplas, Alexandre Passos, David Cournapeau, Matthieu Brucher, Matthieu Perrot, and Édouard Duchesnay, 2011. Scikit-learn: Machine Learning in Python. *Journal of Machine Learning Research*, vol. 12, pp. 2825–2830, (2011). https://doi.org/0.5555/1953048.2078195

[31] Yusuf Aydin, Ozan Tokatli, Volkan Patoglu, and Cagatay Basdogan, 2017. Fractional order admittance control for physical human-robot interaction. *IEEE World Haptics Conference (WHC)*, pp. 257–262, (2017). https://doi.org/10.1109/WHC.2017.7989911

[32] Alireza Madani, Pouya P. Niaz, Berk Guler, Yusuf Aydin, and Cagatay Basdogan, 2022. Robot-Assisted Drilling on Curved Surfaces with Haptic Guidance under Adaptive Admittance Control. *IEEE/RSJ International Conference on Intelligent Robots and Systems (IROS)*, pp. 3723-3730, (2022). https://doi.org/10.48550/arXiv.2207.13999